THE JOURNAL OF PHYSICAL CHEMISTRY C

Article

pubs.acs.org/JPCC

The Role of Defects in the Local Reaction Kinetics of CO Oxidation on Low-Index Pd Surfaces

D. Vogel,[†,‡] C. Spiel,[†] M. Schmid,[§] M. Stöger-Pollach,[⊥] R. Schlögl,[‡] Y. Suchorski,[†,*] and G. Rupprechter[†]

[†]Institute of Materials Chemistry, [§]Institute of Applied Physics, and [⊥]University Service Center for Transmission Electron Microscopy, Vienna University of Technology, Vienna, Austria

[‡]Fritz-Haber-Institut der Max-Planck-Gesellschaft, Berlin, Germany

ABSTRACT: The role of artificially created defects and steps in the local reaction kinetics of CO oxidation on the individual domains of a polycrystalline Pd foil was studied by photoemission electron microscopy (PEEM), mass spectroscopy (MS), and scanning tunneling microscopy (STM). The defects and steps were created by STM-controlled Ar^+ sputtering and the novel PEEM-based approach allowed the simultaneous determination of local kinetic phase transitions on differently oriented μm-sized grains of a polycrystalline sample. The independent (single-crystal-like) reaction behavior of the individual Pd(hkl) domains in the 10^{-5} mbar pressure range changes upon Ar^+ sputtering to a correlated reaction behavior, and the reaction fronts propagate unhindered across the grain boundaries. The defect-rich surface shows also a significantly higher CO tolerance as reflected by the shift of both the global (MS-measured) and the local (PEEM-measured) kinetic diagrams toward higher CO pressure.

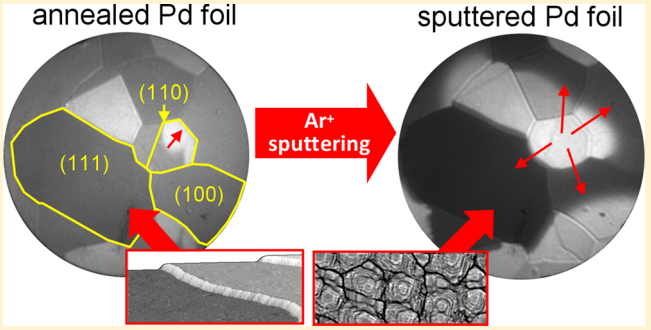

INTRODUCTION

The structure dependence of the reaction rates and the selectivity of heterogeneously catalyzed reactions, as well as the related identification of catalytically "active sites", are among the most discussed topics since the early days of catalysis.[1,2] Atomic steps and surface defects are often considered to be crucial for heterogeneous catalysis,[3−6] since these particular active sites strengthen the reactant-surface binding[7] and thus also facilitate bond formation and breaking.[8]

With respect to the CO oxidation reaction on platinum-group metal surfaces, structure sensitivity has been mainly studied by comparing the reaction kinetics on differently structured single crystal surfaces, measured in independent experiments.[9−12] Despite the obvious drawbacks of such measurements caused by the difficulties to keep the conditions and control parameters exactly the same in separate experiments, important findings, for example, for Pd surfaces, such as significant differences of the CO coverage on differently oriented planes under identical experimental conditions,[9] high structure sensitivity at low coverages, and low sensitivity to the surface orientation at medium or high coverages,[10] and significant dependence of the rate of CO oxidation on the structure-dependent oxygen bond energy were obtained.[11]

For studying the role of atomic steps and defects, basically two types of approaches are usually utilized: (i) either the reaction is studied on vicinal surfaces exhibiting regular steps such as Pt(335)[13] and Pt(332)[14] or (ii) the surface steps and defect sites are intentionally created, for example, by sputtering or laser radiation.[15] Ar^+ ion sputtering is a suitable method to create artificial roughness, since the energy of Ar^+ ions, the Ar^+ ion dose, and the temperature during sputtering allow a flexible variation of the surface topography. For example, the artificial creation of defects by Ar^+ ion sputtering on a Rh surface oxide grown on Rh(111) significantly increased the number of nuclei for oxide reduction by H_2 (i.e., reduction was facilitated by roughness).[16] Nevertheless, if the effect of ion bombardment of various low-index surfaces is examined in separate experiments, the problem of experimental deviations remains.

Recently, we have developed a photoemission electron microscopy (PEEM)-based approach that allows one to study the local reaction kinetics of CO oxidation *in situ* on individual differently oriented micrometer-sized grains of a polycrystalline metal foil.[17−19] Owing to the parallel imaging principle of PEEM, the local kinetic information is obtained simultaneously for all micrograins in the field of view (ca. 500 μm) under exactly the same conditions. If this is extended to the case of Ar^+ ion sputtering, all domains of the polycrystalline sample surface are subject to identical ion impact, and the parallel analyzing method PEEM thus provides a possibility to compare the local kinetics of differently oriented, but similarly Ar^+-"modified" surfaces.

In the present contribution we exploit this possibility, applying digital analysis of PEEM video-sequences recorded *in situ* during the CO oxidation reaction to obtain local kinetic

Received: December 19, 2012
Revised: May 17, 2013
Published: May 17, 2013

   dx.doi.org/10.1021/jp312510d | *J. Phys. Chem. C* 2013, 117, 12054−12060

information from the smooth (sputtered and annealed) and atomically rough (additionally sputtered) surface of individual Pd(*hkl*) domains of a polycrystalline Pd foil. The degree of the surface modification caused by Ar^+ ion impact was estimated by scanning tunneling microscopy (STM) and the global (average) kinetics of the CO oxidation reaction was monitored by mass spectroscopy (MS).

EXPERIMENTAL SECTION

The experiments were performed in a ultra-high-vacuum (UHV) system consisting of two independently operated chambers connected with each other by a sample transfer line, thus allowing a common reactive gas atmosphere in the 10^{-4} to 10^{-9} mbar range. The "microscopy" chamber is equipped with a photoemission electron microscope (PEEM, Staib instruments), a quadrupole mass spectrometer (QMS, MKS instruments), a LEED system (Omicron), a high purity gas supply system (O_2: 99.999%, CO: 99.97%) and sample preparation facilities for cleaning the sample by argon ion sputtering and annealing. The "spectroscopy" chamber is equipped with an XPS-system (Phoibos 100 hemispherical energy analyzer and XR 50 twin anode X-ray source, SPECS). The details of the experimental setup are described elsewhere.[20]

The investigated sample was a polycrystalline Pd foil (AlfaAesar, 99.9% purity) which consisted of 50−100 μm large grains of different crystallographic orientation formed after heating the sample for several hours at 1100 K in UHV. A standard UHV cleaning procedure, namely Ar^+ ion sputtering (Ar pressure 10^{-5} mbar, E_{kin} = 1 keV), annealing at 1073 K and subsequent heating at 523 K in 5 × 10^{-7} mbar oxygen atmosphere, was performed before each measurement. The sample temperature was measured by a NiCr/Ni thermocouple spot-welded to the front side of the Pd sample.

The idea of the experimental approach is illustrated in Figure 1. The global CO_2 formation rate in the CO oxidation reaction, originating from all grains of the Pd foil (Figure 1a), is monitored by QMS yielding the *global* reaction kinetics of this reaction on the whole sample (Figure 1b). Simultaneously, PEEM is applied to visualize the reaction *in situ*. The contrast of a PEEM image which is formed by photoelectrons, emitted from the surface upon UV light illumination, is attributed to the local work function variations across the sample. These variations are sufficient to monitor the CO oxidation reaction. The digital analysis of the recorded video sequences allows one to follow the reaction on the individual grains of the polycrystalline sample and to obtain *local* kinetic transitions on specific domains (Figure 1c).

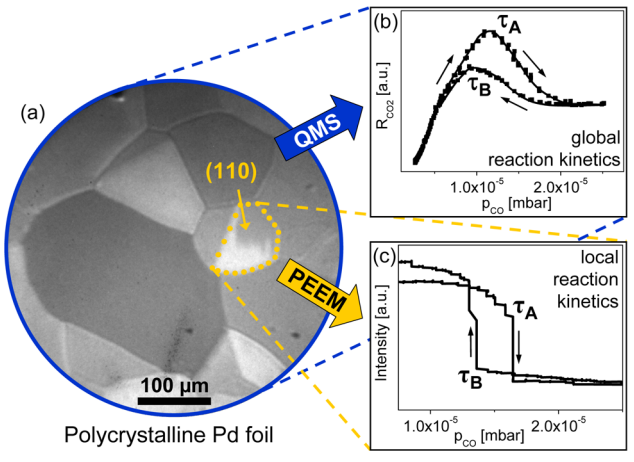

Figure 1. Scheme of the experiment. (a) PEEM image of the polycrystalline Pd sample during the CO oxidation reaction (T = 449 K, p_{CO} = 1.4 × 10^{-5} mbar, p_{O2} = 1.3 × 10^{-5} mbar). (b) Global hysteresis in the overall CO_2 reaction rate measured during a cycle of CO pressure variation at constant T = 449 K and p_{O2} = 1.3 × 10^{-5} mbar by MS for the whole sample. (c) Local hysteresis as obtained from a corresponding PEEM video sequence for the Pd(110) domain indicated in part a; acquired simultaneously with the MS-measurement in part b.

The identification of different grains of a Pd foil by local PEEM image contrast is a challenging task because of the rather small work-function differences of individual orientations. Therefore, electron backscatter diffraction (EBSD) has been applied to determine the crystallographic orientation of the individual grains and to confirm the orientation of those low index facets which was primarily determined by work function analysis by PEEM.

Particular attention was paid to the possibility of palladium oxide formation during the CO oxidation: the possibility to keep a common reactive gas atmosphere in the PEEM- and the XPS-chamber allowed us to perform XPS-measurements under the conditions of the CO oxidation reaction (in the 10^{-5} mbar pressure range). We have not observed any formation of a palladium bulk or surface oxide under the present conditions.

EBSD measurements have been carried out independently in a scanning electron microscope (FEI, Quanta 200F) equipped with an EBSD detector that allows recording of the Kikuchi bands, which provide the EBSD pattern of a given sample spot. Figure 2 shows the resulting orientation map and a comparison

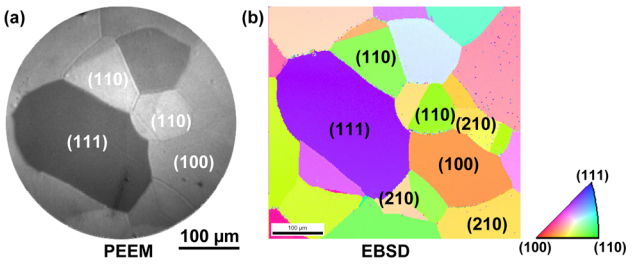

Figure 2. Orientation of the particular surface domains for a chosen field of view of the polycrystalline Pd foil: (a) as identified by work function differences in PEEM; (b) the same, but by EBSD. Note the inverse pole figure assigning the corresponding directions.

with the PEEM image of a clean sample surface. As can be seen from Figure 2, the EBSD results are in perfect agreement with the independent work function analysis by PEEM. The advantage of EBSD is that one can identify also higher Miller index orientations such as, for example, (210) which are often present on the surface, but can hardly be identified on the basis of sole work function measurements. Owing to the unique shape of the individual domains, the domains identified by EBSD can be easily located and visually recognized by PEEM, and the chosen domain of the sample surface can be placed in front of the PEEM lens by the movable sample holder.

The STM experiments on the Pd(111) single crystal have been carried out in a separate UHV system with a base pressure below 10^{-10} mbar in both the preparation and analysis chambers, using the customized commercial STM (Omicron μ-STM) as described elsewhere.[21]

dx.doi.org/10.1021/jp312510d | J. Phys. Chem. C 2013, 117, 12054−12060

RESULTS AND DISCUSSION

Using the above-mentioned combined PEEM–MS approach, a systematic set of kinetic measurements for the CO oxidation reaction on the polycrystalline Pd foil was performed, upon which both the CO_2 reaction rate and the video-PEEM data were recorded simultaneously during a cyclic variation of the CO partial pressure in the range of $\sim 10^{-8}$ mbar to $\sim 10^{-4}$ mbar at constant oxygen pressure ($p_{O2} = 1.3 \times 10^{-5}$ mbar) and different constant temperatures in the range of 405 to 513 K. Both the global CO_2 reaction rate, produced by the entire sample, and the local PEEM intensities of the individual grains exhibit a pronounced hysteresis (see Figure 1b,c).

The observed hysteresis characterizes the bistability in the CO oxidation reaction as an inherent property of a reaction between a strongly bound monomer (CO) and a dimer (O_2) with different adsorption kinetics: O_2 dissociation is blocked on a densely CO-covered surface, while CO can still adsorb and react on a surface with saturation coverage of adsorbed oxygen.[22] Thus, in a range of reaction conditions two states can be stable: a catalytically active surface with high oxygen coverage, where adsorbing CO is quickly removed by the reaction with adsorbed oxygen, as well as a completely CO-covered state of the surface, which is inactive (CO-poisoned).[23,24]

The bistable behavior of the CO oxidation on the platinum group metals is well studied, both experimentally[25−27] and theoretically, where mean field (MF) mesoscopic models[28] and kinetic Monte Carlo (KMS) atomistic models[29,30] were applied. In particular, the pioneering work of Ziff, Gulari, and Barshad should be mentioned because of admitting spatial inhomogeneities usually averaged in mean field considerations.[29] Studies on microscopically sized surfaces like nanofacets of a Pt field emitter tip[31] or clusters[32] have demonstrated that the bistability remains present, as an inherent property of a monomer–dimer Langmuir–Hinshelwood reaction, also in nanosized reaction systems and is limited only by fluctuation-induced effects.[33]

It has been shown that the bistability and kinetic transitions from, for example, active to inactive state have formal similarities to equilibrium phase transitions. As already noticed by Schlögl in the 1970s, in both equilibrium and non-equilibrium phase transitions, a crucial role is played by cooperative phenomena forming, for example, ordered structures in an equilibrium, and self-organizing dissipative structures in a nonequilibrium situation.[34,35] The coverage of the reactants plays here the role of the order parameter in a phase transition, and the point where bistability sets in corresponds to the critical point (bifurcation).[36−38]

The transitions from the active to the inactive state and *vice versa* are called kinetic transition points τ_A and τ_B, respectively (see Figure 1b,c). This means that the behavior of the reaction system changes qualitatively when some externally controlled parameters such as temperature or pressure pass a certain value.[36]

Plotting the p_{CO} of τ_A and τ_B, which were determined from the R_{CO2} hysteresis curves (see Figure 1b), as a function of the reciprocal temperature, yields the so-called kinetic phase diagram, which is presented for the polycrystalline Pd foil in Figure 3. Such a diagram summarizes effectively the steady states of high reactivity and low reactivity as well as the region of bistability and represents the catalytic properties of the *entire sample* in a wide range of p_{CO} and T at constant p_{O2}. Since the transition points depend not only on external parameters as the temperature, but naturally also on intrinsic properties of the studied system such as the crystallographic orientation or the surface structure (roughness), such a diagram characterizing the particular system is well suited to compare different reaction systems and to reveal the influence of different factors such as promoters.[39]

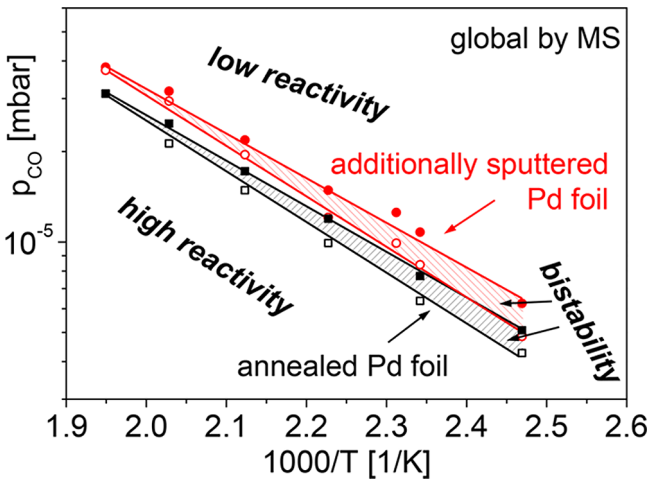

Figure 3. Global kinetic phase diagrams for the smooth (sputtered and annealed) Pd foil (black squares) and for the same but additionally sputtered Pd foil (red circles), as obtained by MS at constant $p_{O2} = 1.3 \times 10^{-5}$ mbar and different constant temperatures in the range between 405 and 513 K. Filled and empty symbols represent the τ_A and τ_B transitions, correspondingly.

The main goal of the present study was to compare the catalytic properties of the nearly ideal, that is, sputtered and annealed Pd(*hkl*) surfaces with the same surfaces that were artificially modified by additional Ar^+ sputtering. In the global kinetic diagrams of the smooth and the sputtered Pd foil, a remarkable difference is apparent (see Figure 3): the diagram for the sputtered foil (red symbols in Figure 3) is shifted significantly toward higher CO pressure, as compared to that of the smooth surface. This indicates that CO oxidation on the sputtered Pd foil is inhibited by CO poisoning only at a considerably higher CO partial pressure and the sputtered surface is also reactivated at a higher CO pressure than the annealed Pd foil. In other words, the defect-rich sputtered sample is much more tolerant toward CO poisoning than the smooth surface.

To explain these observations, STM has been applied to image both a smooth and an additionally sputtered Pd(111) single crystal surface which was subjected to Ar^+ sputtering under the same conditions as the Pd foil (E_{kin} = 1 keV, ion dose 2×10^{16} cm^{-2}, sample at room temperature). The corresponding STM images are shown in Figures 4a,b. The freshly prepared (sputtered and annealed) Pd(111) surface exhibits well-defined smooth terraces with a typical terrace width of 20–30 nm (Figure 4a). The situation changes strongly upon sputtering (Figure 4b): ion bombardment of the surface leads to formation of three-dimensional islands, with a very high density of steps and edges. The uppermost terraces of the mounds have diameters of 2–3 nm, and the slope angles are between 10° and 20°, corresponding to terrace widths of 0.6 to 1.2 nm. This means that about one-quarter of all surface Pd atoms are step or kink atoms. With the *in-plane* lattice constant of the Pd(111) surface of 2.74 Å the surface corresponds to a mixture of high-index surfaces with 2–6 atom wide (111)

dx.doi.org/10.1021/jp312510d | J. Phys. Chem. C 2013, 117, 12054−12060

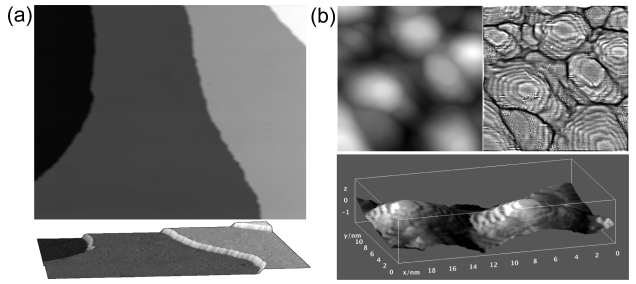

Figure 4. (a) STM micrograph of the annealed Pd(111) surface (100 × 100 nm^2). (b) The same surface after Ar$^+$ ion sputtering (20 × 20 nm^2; the high-pass filtered image on the right shows the steps). The bottom of each panel shows a 3D view; enhancement of high frequencies and edge-preserving blur has been used to improve the visibility of steps in the 3D image (b).

terraces and [100]- and [110]-directed steps, but with an additional very high amount of kink atoms.

It is known that the binding energy of oxygen is considerably higher at low-coordination defect sites than on flat terraces of Pd; that is, atomic oxygen binds more strongly to a defect-rich Pd surface.[40,41] Although the CO binding energy is also altered on such defect sites on the Pd surface,[42] the impact on the CO adsorption kinetics appears to be rather small when compared to oxygen.[43] Since the energetics governs the kinetics of the competitive CO and oxygen coadsorption, this explains why on the sputtered Pd surface higher CO pressure is required to poison the surface. The higher CO pressure values at which reactivation of the sputtered Pd surface occurs, that is, the reverse transition τ_B, can be directly explained by the adsorption kinetics rather than the energetics: Owing to the high step and defect density, more adsorption sites for oxygen adsorption on a mainly CO-covered surface are available, the sticking probability for oxygen adsorption is considerably higher, and, therefore, the reactivation occurs at a higher CO-to-oxygen pressure ratio than on the smooth surface.

Although an illustration of the global catalytic properties such as in Figure 3 is useful, it does not provide any local information about the properties of the individual grains due to the averaging character of the measurement method (MS). In turn, PEEM provides the laterally resolved data. Since the PEEM images and the EBSD scan revealed that the sample consists of many grains with differing crystallographic orientation it could be expected that the effect of sputtering on the catalytic behavior of the individual (hkl) domains could be different (due to the different initial atomic configurations of the grains). As mentioned, the analysis of the local PEEM-intensities for selected individual crystalline grains allows the acquisition of the local hysteresis curves (Figure 1c) which result in turn in the *local kinetic phase diagrams* as shown in Figure 5 for the four chosen (110)-, (210)-, (100)-, and (111)-oriented domains of the smooth Pd surface. As expected for different orientations, the CO-tolerance and the ability for reactivation are clearly related to the atomic structure: whereas the local kinetic phase diagram of the most open structure among the four studied orientations, that is, the (110) domain, is located at the highest CO-to-oxygen pressure ratio, the corresponding diagram of the closest-packed (111) domain is situated at the lowest value of the pressure ratio. In turn, the local kinetic phase diagram of the (210) domain with a surface consisting of (100) terraces and (110) steps, lies exactly between the diagrams of the (110) and the (100) domains.

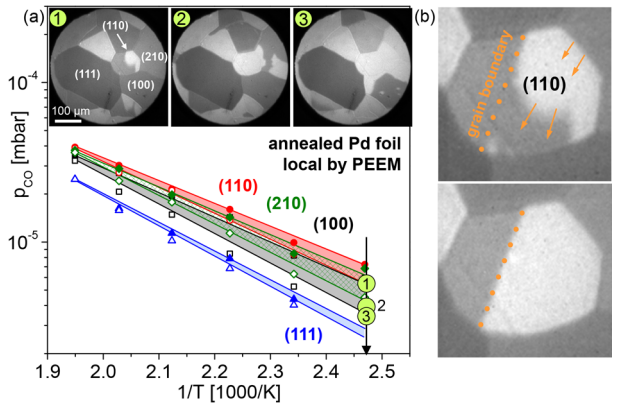

Figure 5. CO oxidation on individual Pd(hkl) domains of a smooth Pd foil. (a) Local kinetic phase diagrams of individual [110]- (red), [210]- (green), [100]- (black), and [111]-oriented (blue) domains of Pd foil during CO oxidation at constant p_{O2} = 1.3 × 10^{-5} mbar obtained by PEEM intensity analysis. Frames 1−3 illustrate the transition τ_B from the inactive steady state (CO-covered, dark contrast) to the active steady state (oxygen-covered, bright contrast) at 405 K, p_{CO} scan from 5.4 × 10^{-5} mbar to 4.0 × 10^{-5} mbar. (b) PEEM images illustrating the independency of the domains in the CO oxidation reaction: the reaction fronts are stopped at the grain boundaries, no coupling between differently oriented grains was observed under the present conditions.

Before discussing the local PEEM data, we note that the work function of Pd(*hkl*) surfaces increases upon CO adsorption by up to 1.2 eV.[44,45] Adsorption of oxygen, in turn, causes an increase in the Pd(*hkl*) work function values by up to 0.8 eV.[45,46] Thus, the regions covered by oxygen appear brighter than the CO-covered regions (in contrary to Pt surfaces where the contrast is inversed).[17,25,47,48]

The PEEM frames 1−3 in Figure 5, corresponding to CO pressures of 5.4 × 10^{-6} mbar, 4.3 × 10^{-6} mbar, and 4.0 × 10^{-6} mbar, illustrate the transition τ_B from the inactive CO-covered (high work function, dark contrast) state to the highly reactive oxygen covered state (lower work function, bright contrast) at 405 K caused by decreasing the CO pressure. During the transition, bright oxygen fronts propagate across the individual domains (the [111], [100], [210], and [110] orientations are denoted in frame 1), remaining in each case strongly confined within the grain boundaries, that is, no front propagation across the boundaries occurs. Note that the transition τ_B observed for the (210) domain (frame 2) occurs exactly between the τ_B transitions on the (110) and the (100) domains (frame 1 and 3, respectively), confirming again the structure−reactivity relation. In Figure 5b, displaying magnified PEEM images of the (110) domain, it is visible how the bright oxygen front nucleates at the grain boundary, that is, in a region of a very high step and defect density, propagates across the domain, and is effectively stopped at the surrounding grain boundaries due to the unsuitable conditions for the transition τ_B on the surrounding grains.

Apparently, the individual domains behave quasi-independently within the complex neighborhood of other differently oriented grains, at least under the current reaction conditions. Such independent single-crystal-like reaction behavior of the individual grains can be understood by considering possible mechanisms of reactive synchronization (coupling) between the different surface regions: at small (nanometer-sized) length scales, diffusion coupling was made responsible for the

synchronization of local transitions.[33] At pressures higher than 10^{-4} mbar, gas-phase coupling provides the synchronization over macroscopic samples,[49,50] and near atmospheric pressure, heat transfer contributes significantly or even dominates spatial coupling.[51,52] Evidently, under the present pressure conditions, the micrometer size of the individual grains is not sufficient to synchronize the kinetic transitions on differently oriented grains via fast CO and oxygen consumption from the gas phase. On the other hand, the grain boundaries seem to hinder effectively the diffusion coupling (frames 1−3 in Figure 5).

Figure 6 illustrates the change of the local reaction properties of the individual domains upon Ar^+ sputtering, showing the

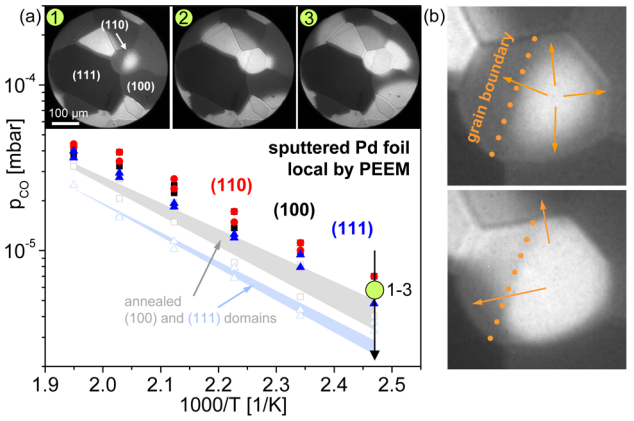

Figure 6. CO oxidation on individual Pd(*hkl*) domains of a sputtered Pd foil. (a) Local kinetic phase diagrams of the individual [110]- (red), [100]- (black), and [111]-oriented (blue) grains on the additionally sputtered Pd foil, in comparison with the (100) and (111) domains on the annealed Pd foil, at constant $p_{O2} = 1.3 \times 10^{-5}$ mbar and different constant temperatures. The local kinetic phase diagrams of the sputtered surface are shifted together and toward higher CO pressures, as compared to the local kinetic phase diagrams of the annealed sample (see Figure 5a). PEEM-frames 1−3: transition τ_B at 405 K on the additionally sputtered Pd foil, $p_{CO} = 5.9 \times 10^{-5}$ mbar. (b) PEEM images illustrating the propagation of the reaction fronts across the grain boundaries. The independency of the individual domains is lifted.

local kinetic phase diagrams of the same (110)-, (100)-, and (111)-oriented domains as in Figure 5, but measured after additional Ar^+ ion bombardment (15 min, 1 keV). For comparison, the local kinetic phase diagrams of the annealed (100) and the (111) domains are included. Evidently, the local kinetic transitions on all domains are now located at generally higher CO pressures, as expected from the global results (Figure 3). In turn, the individual kinetic phase diagrams, which were clearly separated from each other in the case of the smooth foil, are shifted together and can hardly be distinguished from each other for the sputtered foil. This means that the local kinetic transitions on the individual domains of the *sputtered* Pd foil occur almost "at once" and not "delayed" with respect to each other, as we had observed for the smooth surface.

The PEEM frames 1−3 in Figure 6a, recorded within a few seconds at a CO partial pressure of 5.9×10^{-6} mbar, showing the transition τ_B at the same temperature of 405 K as in Figure 5, but on the additionally sputtered sample, confirm this suggestion: The bright oxygen fronts do not stop at the grain boundaries and propagate almost instantaneously across the entire foil. It is clear that on the sputtered Pd foil the differences in the local reaction kinetics are reduced by sputtering, due to the similarly damaged structure of the different domains. Thus, the reaction fronts propagate across the grain boundaries, because the conditions required for the kinetic transition are similar on the now similarly structured neighboring grains. Also, the grain boundaries do not serve as nucleation centers for the reaction fronts anymore, which can be clearly seen by a comparison of the magnified PEEM images of the (110) domain in Figures 5b and 6b. On the additionally sputtered foil, the reaction fronts nucleate primarily in the inner part of the domains rather than at the grain boundaries; that is, the defects on the roughened surface of the sputtered foil are able to nucleate the reaction fronts (Figure 6b). We attribute the nucleation of the reaction fronts at grain boundaries of the unsputtered surface to high-index facets in the grooves separating different grains. In contrast, on the sputtered surface, the local atomic-scale roughness will be high both in the macroscopically flat areas and in the grooves; thus the reaction fronts can start anywhere.

In general, Ar^+ sputtering at the applied intensity apparently creates a similarly "damaged" (roughened) surface structure on all individual low-index Pd domains, lifting in this way their quasi-independent behavior in the CO oxidation and shifting significantly the individual local kinetic phase diagrams. This should enable future applications with a finely dosed impact of Ar^+ ions, creating controlled structure disorder and targeted phase diagram shifts as a step toward tailored catalytic properties. Using of this approach to modify in a controlled way bimetallic or oxide-covered surfaces might be also feasible, of course.

SUMMARY

The role of artificially created defects and steps in the local reaction kinetics of CO oxidation on low-index Pd surfaces was studied by PEEM, MS, and STM. The reaction kinetics on the smooth (Ar^+ sputtered and annealed) and defect-rich (additionally Ar^+ sputtered) Pd(*hkl*) surfaces were directly compared, using the novel PEEM-based approach, allowing the simultaneous determination of local kinetic phase transitions on micrometer-sized grains of a polycrystalline sample.

In the case of the smooth surface, individual Pd(*hkl*) domains behave independently (single-crystal-like) with respect to CO oxidation at the present conditions, that is, in the 10^{-5} mbar pressure range. In turn, after sputtering, the presence of plenty of defects lifts the domain independency and leads rather to a correlated reaction behavior: the kinetic phase diagrams of the different grains approach each other and the reaction fronts propagate unhindered across the grain boundaries. Both the global (MS-measured) and the local (PEEM-measured) kinetic phase diagrams shift toward a higher CO pressure (higher CO tolerance) for the defect-rich surface, due to the differently modified oxygen and CO binding energies on the low-coordinated step and defect sites, as compared to the smooth surface. The exact identity of the experimental conditions for the different crystallographic orientations and the parallel principle of the used PEEM-technique, which allow the simultaneous monitoring of dynamic processes on different domains, open interesting perspectives for future applications of this approach.

AUTHOR INFORMATION

Corresponding Author

*E-mail: yuri.suchorski@imc.tuwien.ac.at. Tel.: +43-1-58801165106.

Notes

The authors declare no competing financial interest.

ACKNOWLEDGMENTS

This work was supported by the Austrian Science Fund (FWF) [SFB F45 FOXSI]. Technical support by Johannes Frank (IMC, TU Vienna) is cordially acknowledged.

REFERENCES

(1) Taylor, H. S. A Theory of the Catalytic Surface. *Proc. R. Soc. London, Ser. A* **1925**, *108*, 105−111.
(2) Nørskov, J. K.; Bligaard, T.; Hvolbæk, B.; Abild-Pedersen, F.; Chorkendorff, I.; Christensen, C. H. The Nature of the Active Site in Heterogeneous Metal Catalysis. *Chem. Soc. Rev.* **2008**, *37*, 2163−2171.
(3) Yates, J. T. Surface Chemistry at Metallic Step Defect Sites. *J. Vac. Sci. Technol. A* **1995**, *13*, 1359−1367.
(4) Zambelli, T.; Wintterlin, J.; Trost, J.; Ertl, G. Identification of the "Active Sites" of a Surface-Catalyzed Reaction. *Science* **1996**, *273*, 1688−1690.
(5) Wandelt, K. Properties and Influence of Surface Defects. *Surf. Sci.* **1991**, *251*−*252*, 387−395.
(6) Rupprechter, G. Sum Frequency Generation and Polarization-Modulation Infrared Reflection Absorption Spectroscopy of Functioning Model Catalysts from Ultrahigh Vacuum to Ambient Pressure. *Adv. Catal.* **2007**, *51*, 133−263.
(7) Hammer, B.; Nielsen, O. H.; Nørskov, J. K. Structure Sensitivity in Adsorption: CO Interaction with Stepped and Reconstructed Pt Surfaces. *Catal. Lett.* **1997**, *46*, 31−35.
(8) Vang, R. T.; Honkala, K.; Dahl, S.; Vestergaard, E. K.; Schnadt, J.; Laegsgaard, E.; Clausen, B. S.; Nørskov, J. K.; Besenbacher, F. Controlling the Catalytic Bond-Breaking Selectivity of Ni Surfaces by Step Blocking. *Nat. Mater.* **2005**, *4*, 160−162.
(9) Szanyi, J.; Goodman, D. W. CO Oxidation on Palladium. 1. A Combined Kinetic-Infrared Reflection Absorption Spectroscopic Study of Pd(100). *J. Phys. Chem.* **1994**, *98*, 2972−2977.
(10) Zhang, C. J.; Hu, P. CO Oxidation on Pd(100) and Pd(111): A Comparative Study of Reaction Pathways and Reactivity at Low and Medium Coverages. *J. Am. Chem. Soc.* **2001**, *123*, 1166−1172.
(11) Santra, A. K.; Goodman, D. W. Catalytic Oxidation of CO by Platinum Group Metals: from Ultrahigh Vacuum to Elevated Pressures. *Electr. Acta* **2002**, *47*, 3595−3609.
(12) Szanyi, J.; Kuhn, W. K.; Goodman, D. W. CO Oxidation on Palladium. 2. A Combined Kinetic-Infrared Reflection Absorption Spectroscopic Study of Pd(111). *J. Phys. Chem.* **1994**, *98*, 2978−2981.
(13) Xu, J.; Yates, J. T. Catalytic Oxidation of CO on Pt(335): A Study of the Active Site. *J. Chem. Phys.* **1993**, *99*, 725−732.
(14) Wang, J. G.; Li, W. X.; Borg, M.; Gustafson, J.; Mikkelsen, A.; Pedersen, T. M.; Lundgren, E.; Weissenrieder, J.; Klikovits, J.; Schmid, M.; et al. One-Dimensional PtO_2 at Pt Steps: Formation and Reaction with CO. *Phys. Rev. Lett.* **2005**, *95*, 256102.
(15) Castell, R.; Reiff, S.; Drachsel, W.; Block, J. H. Influence of Laser-Induced Defects on Catalytic CO Oxidation on Pt(111). *Surf. Sci.* **1997**, *377*−*379*, 770−774.
(16) Klikovits, J.; Schmid, M.; Gustafson, J.; Mikkelsen, A.; Resta, A.; Lundgren, E.; Andersen, J. N.; Varga, P. Kinetics of the Reduction of the Rh(111) Surface Oxide: Linking Spectroscopy and Atomic-Scale Information. *J. Phys. Chem. B* **2006**, *110*, 9966−9975.
(17) Suchorski, Y.; Spiel, C.; Vogel, D.; Drachsel, W.; Schlögl, R.; Rupprechter, G. Local Reaction Kinetics by Imaging: CO Oxidation on Polycrystalline Platinum. *ChemPhysChem* **2010**, *11*, 3231−3235.
(18) Vogel, D.; Spiel, C.; Suchorski, Y.; Urich, A.; Schlögl, R.; Rupprechter, G. Mapping the Local Reaction Kinetics by PEEM: CO Oxidation on Individual (100)-Type Grains of Pt Foil. *Surf. Sci.* **2011**, *605*, 1999−2005.
(19) Vogel, D.; Spiel, C.; Suchorski, Y.; Trinchero, A.; Schlögl, R.; Grönbeck, H.; Rupprechter, G. Local Catalytic Ignition during CO Oxidation on Low-Index Pt and Pd Surfaces: A Combined PEEM, MS, and DFT Study. *Angew. Chem., Int. Ed.* **2012**, *51*, 10041−10044.
(20) Vogel, D.; Budinska, Z.; Spiel, C.; Schlögl, R.; Suchorski, Y.; Rupprechter, G. Silicon Oxide Surface Segregation in CO Oxidation on Pd: An in Situ PEEM, MS and XPS Study. *Catal. Lett.* **2013**, *143*, 235−240.
(21) Klikovits, J.; Napetschnig, E.; Schmid, M.; Seriani, N.; Dubay, O.; Kresse, G.; Varga, P. Surface Oxides on Pd(111): STM and Density Functional Calculations. *Phys. Rev. B* **2007**, *76*, 045405.
(22) Ertl, G. Reactions at Surfaces: From Atoms to Complexity (Nobel Lecture). *Angew. Chem., Int. Ed.* **2008**, *47*, 3524−3535 and references therein.
(23) Ehsasi, M.; Berdau, M.; Rebitzki, T.; Charlé, K.-P.; Christmann, K.; Block, J. H. A Reactive Phase Diagram of CO Oxidation on Pd(110): Steady and Oscillatory States. *J. Chem. Phys.* **1993**, *98*, 9177−9184.
(24) Zhdanov, V.; Kasemo, B. Steady-State Kinetics of CO Oxidation on Pt: Extrapolation from 10^{-10} to 1 bar. *Appl. Surf. Sci.* **1994**, *74*, 147−164.
(25) Berdau, M.; Yelenin, G. G.; Karpowicz, A.; Ehsasi, M.; Christmann, K.; Block, J. H. Macroscopic and Mesoscopic Characterization of a Bistable Reaction System: CO Oxidation on Pt(111) Surface. *J. Chem. Phys.* **1999**, *110*, 11551−11573.
(26) Suchorski, Y.; Wrobel, R.; Becker, S.; Strzelczyk, B.; Drachsel, W.; Weiss, H. Ceria Nanoformations in CO Oxidation on Pt(111): Promotional Effects and Reversible Redox Behaviour. *Surf. Sci.* **2007**, *601*, 4843−4848.
(27) Karpitschka, S.; Wehner, S.; Küppers, J. Reaction Hysteresis of the CO + O → CO_2 Reaction on Palladium (111). *J. Chem. Phys.* **2009**, *130*, 054706.
(28) Hayase, Y.; Wehner, S.; Küppers, J.; Brand, H. R. External Noise Imposed on the Reaction-Diffusion System CO + O_2 → CO_2 on Ir(111) Surfaces: Experiment and Theory. *Phys. Rev. E* **2004**, *69*, 021609.
(29) Ziff, R. M.; Gulari, E.; Barshad, Y. Kinetic Phase Transitions in an Irreversible Surface- Reaction Model. *Phys. Rev. Lett.* **1986**, *56*, 2553−2556.
(30) Zhdanov, V. P.; Kasemo, B. Bistability in Catalytic Reactions on the nm Scale. *Surf. Sci.* **2002**, *496*, 251−263.
(31) Gorodetskii, V.; Drachsel, W.; Block, J. H. Imaging the Oscillating CO-Oxidation on Pt-Surfaces with Field Ion Microscopy. *Catal. Lett.* **1993**, *19*, 223−231.
(32) Johánek, V.; Laurin, M.; Grant, A. W.; Kasemo, B.; Henry, C. R.; Libuda, J. Fluctuations and Bistabilities on Catalyst Nanoparticles. *Science* **2004**, *304*, 1639−1644.
(33) Suchorski, Y.; Beben, J.; James, E. W.; Evans, J. W.; Imbihl, R. Fluctuation-Induced Transitions in a Bistable Surface Reaction: Catalytic CO Oxidation on a Pt Field Emitter Tip. *Phys. Rev. Lett.* **1999**, *82*, 1907−1910.
(34) Schlögl, F. On Thermodynamics Near a Steady State. *Z. Phys.* **1971**, *248*, 446−458.
(35) Schlögl, F. Chemical Reaction Models for Non-equilibrium Phase Transitions. *Z. Phys.* **1972**, *253*, 147−161.
(36) Zhdanov, V. P.; Kasemo, B. Kinetic Phase Transitions in Simple Reactions on Solid Surfaces. *Surf. Sci. Rep.* **1994**, *20*, 113−189.
(37) Bykov, V. I.; Elokhin, V. I.; Gorban, A. N.; Yablonskii, G. S. *Kinetic Models of Catalytic Reactions*; Vol. *32* of Comprehensive Chemical Kinetics; Elsevier: Amsterdam, 1991.
(38) Suchorski, Y.; Beben, J.; Imbihl, R.; James, E. W.; Da-Jiang, Liu; Evans, J. W. Fluctuations and Critical Phenomena in Catalytic CO Oxidation on Nanoscale Pt Facets. *Phys. Rev. B* **2001**, *63*, 165417.
(39) Suchorski, Y.; Wrobel, R.; Becker, S.; Weiss, H. CO Oxidation on a CeO_x/Pt(111) Inverse Model Catalyst Surface: Catalytic Promotion and Tuning of Kinetic Phase Diagrams. *J. Phys. Chem. C* **2008**, *112*, 20012−20017.

(40) Zhang, Y.; Rogal, J.; Reuter, K. Density-Functional Theory Investigation of Oxygen Adsorption at Pd(11N) Vicinal Surfaces (N = 3,5,7): Influence of Neighboring Steps. *Phys. Rev. B* **2006**, *74*, 125414.
(41) Westerström, R.; Gustafson, J.; Resta, A.; Mikkelsen, A.; Andersen, J. N.; Lundgren, E.; Seriani, N.; Mittendorfer, F.; Schmid, M.; Klikovits, J.; et al. Oxidation of Pd(553): From Ultrahigh Vacuum to Atmospheric Pressure. *Phys. Rev. B* **2007**, *76*, 155410.
(42) Yudanov, I. V.; Sahnoun, R.; Neyman, K. M.; Rösch, N.; Hoffmann, J.; Schauermann, S.; Johanek, V.; Unterhalt, H.; Rupprechter, G.; Libuda, J.; et al. CO Adsorption on Pd Nanoparticles: Density Functional and Vibrational Spectroscopy Studies. *J. Phys. Chem. B* **2003**, *107*, 255−264.
(43) Ramsier, R. D.; Lee, K.-W.; Yates, J. T. CO Adsorption on Stepped Pd(112): Studies by Thermal and Electron Stimulated Desorption. *Surf. Sci.* **1995**, *322*, 243−255.
(44) Conrad, H.; Ertl, G.; Koch, J.; Latta, E. E. Adsorption of CO on Pd Single Crystal Surfaces. *Surf. Sci.* **1974**, *43*, 462−480.
(45) He, J.-W.; Memmert, U.; Griffiths, K.; Lennard, W.; Norton, P. Absolute Coverages for the Various Surface Phases of CO and O Adsorbed on Pd(110). *Surf. Sci.* **1988**, *202*, L555−L558.
(46) Surnev, L.; Bliznakov, G.; Kiskinova, M. Oxygen Adsorption on a Pd(111) Surface. *Surf. Sci.* **1984**, *140*, 249−260.
(47) Ertl, G. Oscillatory Kinetics and Spatio-Temporal Self-Organization in Reactions at Solid Surfaces. *Science* **1991**, *254*, 1750−1755.
(48) Lauterbach, J.; Rotermund, H. H. Spatio-Temporal Pattern Formation during the Catalytic CO-Oxidation on Pt(100). *Surf. Sci.* **1994**, *311*, 231−246.
(49) Ehsasi, M.; Frank, O.; Block, J. H.; Christmann, K. Coupled Chemical Oscillators on Catalytic Oxidation of CO on Pd(110) Surfaces. *Chem. Phys. Lett.* **1990**, *165*, 115−119.
(50) Sander, M.; Imbihl, R.; Schuster, R.; Barth, J. V.; Ertl, G. Microfacetting of Pt(210) Induced by Oxygen Adsorption and by Catalytic CO Oxidation. *Surf. Sci.* **1992**, *271*, 159−169.
(51) Yamamoto, S. Y.; Surko, C. M.; Maple, M. B. Spatial Coupling in Heterogeneous Catalysis. *J. Chem. Phys.* **1995**, *103*, 8209−8216.
(52) Slinko, M. M.; Ukharskii, A. A.; Jaeger, N. I. Global and Non-Local Coupling in Oscillating Heterogeneous Catalytic Reactions: The Oxidation of CO on Zeolite Supported Palladium. *Phys. Chem. Chem. Phys.* **2001**, *3*, 1015−1021.